Biochimica et Biophysica Acta 1787 (2009) 242–251

Contents lists available at ScienceDirect

Biochimica et Biophysica Acta

journal homepage: www.elsevier.com/locate/bbabio

Assembly of subunit *d* (Vma6p) and G (Vma10p) and the NMR solution structure of subunit G (G_{1-59}) of the *Saccharomyces cerevisiae* V_1V_O ATPase

Sankaranarayanan Rishikesan [a], Shovanlal Gayen [a], Youg R. Thaker [a], Subramanian Vivekanandan [a,b], Malathy S.S. Manimekalai [a], Yin Hoe Yau [a], Susana Geifman Shochat [a], Gerhard Grüber [a,*]

[a] *School of Biological Sciences, Nanyang Technological University, 60 Nanyang Drive, Singapore 637551, Republic of Singapore*
[b] *Structural Biology/NMR Spectroscopy, CBER/FDA, NIH campus, Bethesda, MD 20892, USA*

ARTICLE INFO

Article history:
Received 9 September 2008
Received in revised form 12 January 2009
Accepted 13 January 2009
Available online 22 January 2009

Keywords:
Vacuolar-type ATPase
V_1V_O ATPase
Subunit *d*
Subunit G
Subunit E
Vma6p
Vma7p
Vma10p

ABSTRACT

Understanding the structural traits of subunit G is essential, as it is needed for V_1V_O assembly and function. Here solution NMR of the recombinant N- (G_{1-59}) and C-terminal segment (G_{61-114}) of subunit G, has been performed in the absence and presence of subunit *d* of the yeast V-ATPase. The data show that G does bind to subunit *d* via its N-terminal part, G_{1-59} only. The residues of G_{1-59} involved in *d* binding are Gly7 to Lys34. The structure of G_{1-59} has been solved, revealing an α-helix between residues 10 and 56, whereby the first nine- and the last three residues of G_{1-59} are flexible. The surface charge distribution of G_{1-59} reveals an amphiphilic character at the N-terminus due to positive and negative charge distribution at one side and a hydrophobic surface on the opposite side of the structure. The C-terminus exhibits a strip of negative residues. The data imply that G_{1-59}–*d* assembly is accomplished by hydrophobic interactions and salt-bridges of the polar residues. Based on the recently determined NMR structure of segment E_{18-38} of subunit E of yeast V-ATPase and the presently solved structure of G_{1-59}, both proteins have been docked and binding epitopes have been analyzed.

1. Introduction

Vacuolar-type H^+-ATPases (V_1V_O ATPase, V-ATPase) are evolutionary conserved multimeric complexes that mediate the luminal acidification of various organelles such as yeast and plant vacuoles, endosomes, lysosomes, and clathrin-coated vesicles [1]. Besides this function the enzyme is also described to be responsible for sensing and/or measuring the intravesicular pH, and subsequently transmitting this information from the vesicle lumen to the cytosolic side of the membrane [2]. The V_1V_O ATPase is composed of a water-soluble V_1 ATPase and an integral membrane subcomplex, V_O. ATP is hydrolyzed on the V_1 headpiece consisting of an A_3:B_3 hexamer and the energy released during that process is transmitted to the membrane-bound V_O domain, to drive the ion translocation [3,4]. This energy-coupling occurs via the so-called "stalk" structure, an assembly of the V_1 and V_O subunits C, D, E, F, G, H and subunit *a* as well as *d*, respectively, that forms the functional and structural interface [5]. The V_O domain contains five different subunits in a stoichiometry of a_1:d_1:c_{4-5}:c'_1:c''_1 [6]. The V_O complex can be subdivided into two parts, which are proposed to rotate relative to each other, the peripheral stalk and the proton-translocating ring [7]. The V_O part of the peripheral stalk consists of the N-terminal part of subunit *a* [8] and subunit *d* [9]. The proton-translocating ring comprises the subunits *c*, *c′* and *c″* [6]. The fifth V_O subunit, subunit *d*, has a boxing glove-shape in solution, made-up of two distinct domains [9]. This protein has been proposed to play a role in coupling ATP cleavage and proton transport [10] and is also essential for embryonic development [11]. The *d* subunit is exposed on the cytoplasmic side of the membrane [12], interacting with subunit *a* [13] and G, as found by precipitation assays [14]. The latter one, subunit G, has a copy number of two [15] to three [16] inside the enzyme complex and has been determined to be elongated [17]. Recently it has been observed that at least one G subunit interacts via its N-terminus [18] with the N-terminal segment of subunit E [14,18,19].

We have turned our attention to examine the interaction of subunit *d* and G and to determine the amino acids of subunit G involved in its association with subunit *d*, using the recombinant N- and C-terminal segments, G_{1-59} and G_{61-114} (Fig. 1), respectively, combined with magnetic resonance spectroscopy. Surface plasmon resonance was performed to substantiate the binding results and measure the binding affinity between subunit *d* and subunit G_{1-59}. The three dimensional solution structure of the N-terminal segment G_{1-59}, involved in subunit G and *d* assembly, has been solved by NMR spectroscopy.

* Corresponding author. Tel.: +65 6316 2989; fax: +1 65 6791 3856.
E-mail address: ggrueber@ntu.edu.sg (G. Grüber).

0005-2728/$ – see front matter © 2009 Elsevier B.V. All rights reserved.
doi:10.1016/j.bbabio.2009.01.010

2. Materials and methods

2.1. Biochemicals

ProofStart™ DNA Polymerase and Ni^{2+}-NTA-chromatography resin were received from Qiagen (Hilden, Germany); restriction enzymes were purchased from Fermentas (St. Leon-Rot, Germany). Chemicals for gel electrophoresis were received from Serva (Heidelberg, Germany). Bovine serum albumin was purchased from GERBU Biochemicals (Heidelberg, Germany). $(^{15}NH_4)_2SO_4$ and (^{13}C) glucose were purchased from Cambridge Isotope Laboratories (Andover, U.S.A.). All other chemicals were at least of analytical grade and received from BIOMOL (Hamburg, Germany), Merck (Darmstadt, Germany), Roth (Karlsruhe, Germany), Sigma (Deisenhofen, Germany), or Serva (Heidelberg, Germany).

2.2. Protein production and purification

The recombinant proteins G_{1-59} as well as G_{61-114} and subunit *d* (Vma6p) of the *S. cerevisiae* V-ATPase were produced in *Escherichia coli* BL21 (DE3) cells and purified as described by Rishikesan et al. [18] and Thaker et al. [9], respectively. The uniformly, ^{15}N- and ^{15}N/^{13}C-labeled G_{1-59} and G_{61-114} were expressed in *E. coli* BL21 (DE3) cells using M9 minimal media containing $^{15}NH_4Cl$ or $^{15}NH_4Cl$ plus [U–^{13}C]-glucose. To induce production of proteins, cultures were supplemented with isopropyl-β-D-thio-galactoside (IPTG) to a final concentration of 1 mM. Following incubation for another 4 h at 30 °C, the cells were harvested at 8000 ×*g* for 15 min, 4 °C. Subsequently, all cells were lysed on ice by sonication for 3×1 min in appropriate buffer, G_{1-59} in buffer A (50 mM HEPES, pH 7.0, 150 mM NaCl, 1 mM DTT 1 mM PMSF), and G_{61-114} in buffer B (50 mM HEPES, pH 7.5, 150 mM NaCl, 1 mM DTT, 1 mM PMSF). The lysate was cleared by centrifugation at 10 000 ×*g* for 30 min at 4 °C, the supernatant was passed through a filter (0.45 μm pore-size) and supplemented with Ni^{2+}-NTA resin. The His-tagged protein was allowed to bind to the matrix for 2 h at 4 °C by mixing on a sample rotator (Neolab), and eluted with an imidazole-gradient (25 mM–250 mM) in buffer A and B, respectively. Fractions containing His-tagged proteins were identified by SDS-PAGE [20], pooled and concentrated using Centriprep YM-3 or YM-5 (5 kDa molecular mass (MM) cut off) spin concentrators (Millipore) and subsequently applied on a gel filtration column Superdex HR75 (10/30, Amersham Biosciences). Selected fractions were concentrated in 3 kDa cut off centricon. The purity of the protein sample was analyzed by SDS-PAGE [20]. The SDS-gels were stained with Coomassie Brilliant Blue R250.

2.3. NMR data collection and processing

The NMR sample, G_{1-59} or G_{61-114} was prepared in 90% H_2O/10% D_2O containing 25 mM NaH_2PO_4 (pH 6.8), and 0.1% NaN_3. All NMR experiments were performed at 288 K on a Bruker Avance 600 MHz spectrometer. The experiments recorded on ^{15}N/^{13}C-labeled sample were HNCO, HNCACO, CBCA(CO)NH, HNCACB, 3D ^{15}N-NOESY-HSQC and 3D ^{13}C-NOESY-HSQC. The 3D ^{15}N-NOESY-HSQC and 3D ^{13}C-NOESY-HSQC used mixing time of 200 ms. All the two- and three-dimensional experiments made use of pulsed-field gradients for coherence selection and artifact suppression, and utilized gradient sensitivity enhancement schemes. Quadrature detection in the indirectly detected dimensions was achieved using either the States/TPPI (time-proportional phase incrementation) or the echo/anti-echo method. Baseline corrections were applied wherever necessary. The proton chemical shift was referenced to the methyl signal of DSS (2, 2-dimethyl-2-silapentane-5-sulphonate (Cambridge Isotope Laboratories) as an external reference to 0 ppm. The ^{13}C and ^{15}N chemical shifts were referenced indirectly to DSS. All the NMR data were processed using Bruker Avance spectrometer in-built software Topspin2.1 version. Peak-picking and data analysis of the Fourier transformed spectra were performed with the SPARKY program [21].

2.4. NMR titration experiments

To analyze the binding between subunits G_{1-59}–*d*, and G_{61-114}–*d* a series of ^1H–^{15}N heteronuclear single quantum coherence (HSQC) spectra were recorded at 288 K for the fixed concentration of 100 μM of G_{1-59}, titrated with increasing amounts (up to 1.87 mM) of subunit *d* or with 100 μM of G_{61-114} mixed with increasing amounts of subunit *d*. The proteins were incubated for 30 min for binding during each step of the experiment. The amide ^1H and ^{15}N chemical shifts and intensities of uniformly ^{15}N-labeled sample of G_{1-59} were monitored before and after the addition of an equimolar amount of an unlabeled *d* subunit. The changes observed for the G_{1-59} amide ^1H and ^{15}N chemical shifts were residue-specific reductions in the resonance intensities, with no significant changes observed for the resonance frequencies. All the samples used were either finally dissolved in or exchanged with the buffer, composed of 20 mM Tris/HCl (pH 8.0) and 100 mM NaCl prior to the binding experiments.

2.5. NMR spectroscopy and structure calculation of G_{1-59}

The additional His-tag residues at the N-terminus of G_{1-59}, which are essentially unstructured, were not used in the structure

(A)

```
1   msqkngiatl lqaekeahei vskarkyrqd klkqaktdaa keidsykiqk dkelkefeqk  60
61  naggvgelek kaeagvggel aeikkiaekk kddvvkilie tvikpsaevh inal        114
```

(B)

```
1   megvyfnidn gfiegvvrgy rngllsnnqy inltqcdtle dlklqlsstd ygnflssvss  60
61  eslttsliqe yassklyhef nyirdqssgs trkfmdyity gymidnvalm itgtihdrdk 120
121 geilqrchpl gwfdtlptls vatdleslye tvlvdtplap yfkncfdtae elddmnieii 180
181 rnklykayle dfynfvteei pepakecmqt llgfeadrrs inialnslqs sdidpdlksd 240
241 llpnigklyp latfhlaqaq dfegvraala nvyeyrgfle tgnledhfyq lemelcrdaf 300
301 tqqfaistvw awmkskeqev rnitwiaeci aqnqrerinn yisvy                 345
```

Fig. 1. Amino acid sequence of subunit G (A) and *d* (B), respectively, of the V-ATPase from yeast. The amino acid sequence of G_{1-59} and G_{61-114} are highlighted in gray and black, respectively.

calculation. The structure calculation was performed from the first methionine in the N-terminal which is after the proline residue. The sequential assignments were achieved using triple-resonance backbone experiments (HNCO, HNCACO, HNCACB and CBCA(CO)NH) and all the side chain assignments were done using HCCCONH and (H)CCCONH experiments. Dihedral angle restraints were calculated from H^{α}, C^{α} and CO chemical shifts by using PREDITOR [22]. The distance constraints for the structure calculation were collected from 3D ^{1}H–^{15}N NOESY-HSQC and 3D ^{1}H–^{13}C NOESY-HSQC by manually and automatically assigned NOE using CYANA 3.0 [23,24]. Seven cycles of automated NOESY assignment using the CYANA 3.0 package were performed. In the final CYANA cycle NOESY cross peaks were assigned unambiguously, leading to 565 meaningful NOE distance restraints. 10 conformers of the monomeric G_{1-59} were calculated based on the obtained dihedral angles and NOE restraints. The program MOLMOL was used to visualize the result of ensemble of minimized conformers [24].

2.6. Relaxation measurements

T_1 and T_2 spectra were recorded with spectral widths of 9615.85 Hz sampled over 2048 complex points in the ω_2 (^{1}H) dimension and 2405.12 Hz over 128 complex points in the ω_1 (^{15}N) dimension with 16 scans for each increment in the indirect dimension. The relaxation delay for both T_1 and T_2 measurements was 3.0 s. For T_1 measurements, the spectra were collected with relaxation delays of 5, 20, 40, 60, 80, 130, 210, 330, 400, 470, 630, 800 and 1000 ms, with repeat experiments at 40 and 130 ms for error estimations. Experimental data for T_2 were acquired with delays of 7.2, 14.4, 21.6, 28.8, 43.2, 57.6, 72, 86.4, 93.6, 115.2, 129.2 and 144 ms with duplicate points at 21.6 and 72.0 ms. The delay between 180

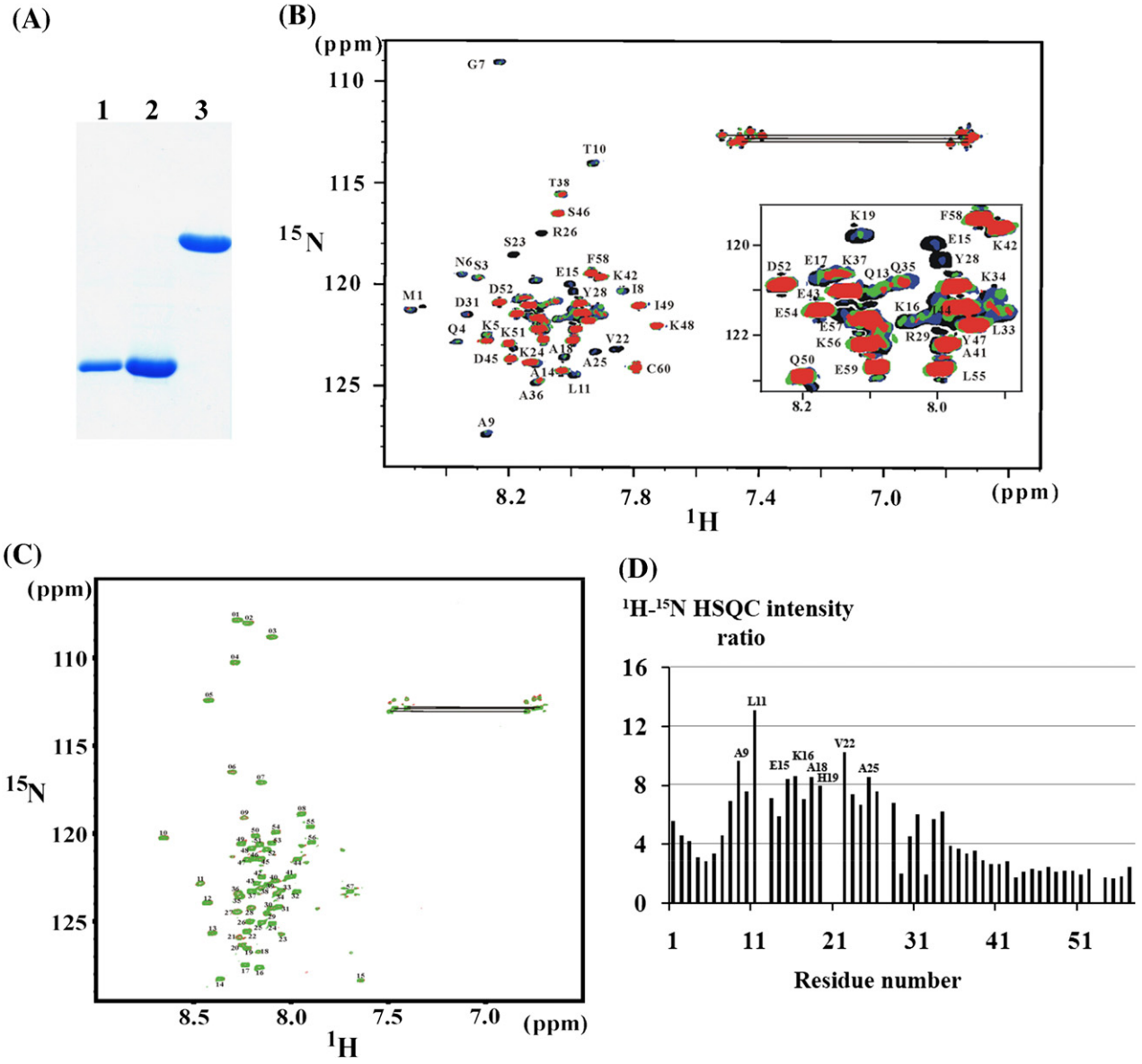

Fig. 2. Titration series of ^{15}N labeled G_{1-59} and G_{61-114} with unlabeled *d* subunit. (A) The SDS-gel shows the produced and purified G_{1-59} (lane 1), G_{61-114} (lane 2) and subunit *d* (lane 3) of the *S. cerevisiae* V-ATPase. (B) The $^{1}H/^{15}N$ HSQC spectra of G_{1-59} are colored as follows: concentration of unlabeled *d* subunit 0 mM (black), 0.125 mM (blue), 0.159 (green) and 0.187 (red). The concentration of G_{1-59} was adjusted to 0.15 mM in all samples. (C) Overlaid $^{1}H/^{15}N$-HSQC spectra of G_{61-114} in the absence (red) and presence (green) of 1.5 equivalents of subunit *d*. (D) Loss of ^{1}H–^{15}N HSQC peak intensity upon titration of unlabeled *d* subunit to ^{15}N-labeled G_{1-59} at a molar ratio of 0.5. The stronger the decrease of the peak intensity compared with the spectrum without *d* subunit, the higher the plotted intensity ratio.

pulses in the Carr–Purcell–Meiboom–Gill (CPMG) pulse train for T_2 measurements was fixed at 0.9 ms. A total of 2048 complex data points with 128 complex increments were collected for the relaxation experiments. The relaxation rate constants were determined by fitting the cross-peak intensities to a mono exponential function.

2.7. CD spectroscopy of G_{1-59}

Steady state CD spectra of G_{1-59} (2.0 mg/ml) were measured in the far UV-light (190–260 nm) using a CHIRASCAN spectropolarimeter (Applied Photophysics). Spectra were collected in a 60 µl quartz cell (Hellma) at 18 °C at a step resolution of 1 nm. The spectrum for the buffer was subtracted from the spectrum of G_{1-59}. This baseline corrected spectrum was used as input for computer methods to obtain predictions of secondary structure.

2.8. Measurement of binding affinities using surface plasmon resonance

Binding affinity of G_{1-59} with subunit *d* of V-ATPase was determined by surface plasmon resonance (SPR) at 25 °C using a Biacore 3000 instrument (BiacoreGE Healthcare, Sweden). Subunit *d* was covalently immobilized on a carboxymethylated sensor surface (CM5, research grade) using amine coupling chemistry [25]. The surfaces were activated with 0.2 M EDC (N-ethyl-N′-[3-(diethylamino) propyl] carbodiimide) and 50 mM NHS, (N-hydroxysuccinimide) for 7 min. The subunit *d* protein was coupled to the desired levels in 10 mM sodium acetate buffer, pH 4.0 and deactivation of the surface was performed using 1 M ethanolamine–HCl (pH 8.5) for 7 min, at a flow-rate of 10 µl/min. The surfaces were checked to ensure that there was no mass-transport limitation for the interaction by monitoring the interaction at different flow-rates. The reference surface was treated as the ligand surfaces except that protein injection was omitted. For the determination of kinetic parameters, G_{1-59} was passed above the reference and protein surfaces in duplicates of five to seven concentrations (3–100 nM), in 10 mM HEPES buffer, pH 7.4, 150 mM KCl, 3.4 mM EDTA and 0.005% P-20, at a flow rate of 30 µl/min. Surfaces were regenerated with a 30 s injection of 50 mM NaOH. Binding experiments were repeated three times. Sensorgrams were fitted using the simple 1:1 Langmuir binding fit model, the association rate constant (k_a) and dissociation rate constant (k_d) were fitted globally by rate Eq. (1), and the equilibrium dissociation rate constant (K_D) was calculated according to Eq. (2). The BIAevaluation 4.1 software was used for data analysis.

$$dR/dt = k_a \times C \times (R_{max} - R) - k_d \times R \quad (1)$$

whereas *C* is the concentration of the analyte and *R* is the response (RU).

$$K_D = k_d / k_a. \quad (2)$$

2.9. Modeling of the interacting domain of NMR structures of G_{1-59} and E_{18-39}

Three best models from the NMR structure of G_{1-59} were chosen for docking studies with the average NMR structure of E_{18-38} peptide which was determined recently [18]. The web interface of the protein docking software GRAMM [26] was used for the docking studies. GRAMM does a global search using the Fast Fourier Transform methodology to identify the best rigid body conformations between the two proteins. Fifty best complex configurations were analyzed for each of the three chosen NMR models of G_{1-59}. These best configurations were scored in GRAMM based on soft Lennard–Jones potential, evolutionary conservation of predicted interface, statistical residue–residue preference, volume of the minimum, empirical binding free energy and atomic contact energy. From these 150 complex configurations the best docking model was chosen in such a way that the model should have almost all residues that show shift in NMR HSQC spectrum [18], and has some kind of interaction in the complex. The subunits G_{1-59}, E_{18-38} and the docked complex were optimized using the program Swiss-PdbViewer 3.7 [27] by carrying out energy minimization *in vacuo* with the GROMOS96 43B1 parameter set, without reaction field as implemented in the program. For fast energy convergence initially 200 steps of Steepest Descent protocol was carried out followed by multiple steps of Conjugate Gradient technique until the derivative convergences to 0.050 kJ/mol.

3. Results

3.1. Binding of subunit d with G_{1-59}

Precipitation assays of GST-tagged subunit G (Vma10p) with recombinant subunit *d* revealed that both subunits do interact with each other [14]. Hitherto, the amino acids inside the stalk subunit G,

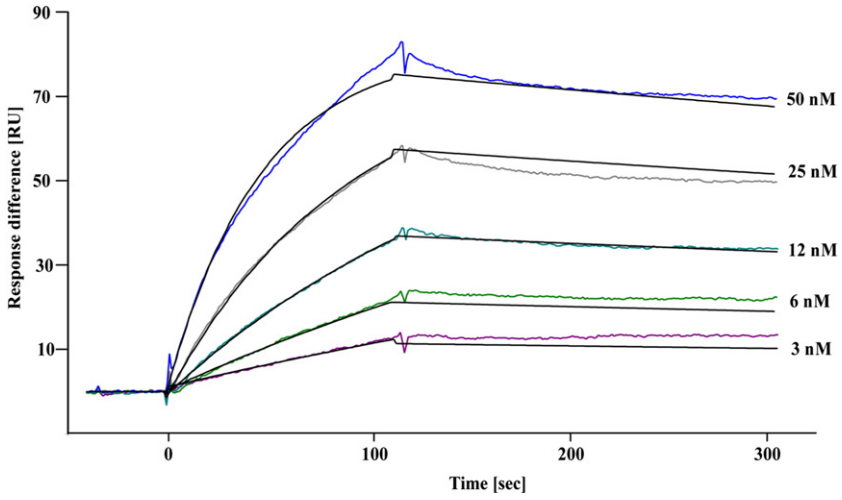

Fig. 3. Real time binding kinetics by surface plasmon resonance. Kinetics of subunits *d* and G_{1-59} binding performed in 10 mM HEPES buffer containing 3.4 mM EDTA, 150 mM KCl and 0.005% P-20, by passing ligand G_{1-59} in duplicates of 3.125, 6.25, 12.5, 25, 50 nM concentrations over the immobilized subunit *d* sensor surface. The sensorgrams were fitted using the Langmuir 1:1 model of BIAevaluation software 4.1.

responsible for the G–*d* formation, have remained undefined. Recently, we demonstrated by NMR spectroscopy that the recombinant N- and C-terminal parts, G_{1-59} (8.0 kDa) and G_{61-114} (7.0 kDa), of subunit G from *S. cerevisiae* V-ATPase enabled to map amino acid residues, involved in subunit G and E association [18]. To assign the amino acid residues of subunit G involved in the subunit G and *d* assembly a series of $^{1}H–^{15}N$ heteronuclear single quantum coherence (HSQC) spectra of ^{15}N-labeled G_{1-59} and G_{61-114} in the presence and absence of recombinant subunit *d* (40.6 kDa; [9]) have been performed (Fig. 2B and C). As shown in Fig. 2B only N-terminal regions of amide resonances of the free G_{1-59} subunit were weakened progressively upon the addition of increasing amounts of *d* subunit. Binding of *d* subunit induces a structural change in the G_{1-59}, which is in chemical exchange on an intermediate rate, with respect to the NMR timescale. This causes broadening or loss of NMR signals in the resonances affected by the binding. These observed phenomena are indicative of complex formation and result from the formation of either a stable, large molecular weight complex or a complex with an exchange rate between the free and bound forms that is similar to the chemical shift difference [28]. Local motions and the degree of separation between the chemical shifts of the free and the bound form of G_{1-59} could also influence the observed loss in signal intensity. By comparison, when equimolar amounts of subunit *d* were added to the ^{15}N-labeled C-terminal segment of subunit G, G_{61-114}, no significant changes either in the chemical shift or in the intensity of the peaks could be detected in the $^{1}H–^{15}N$ HSQC spectrum (Fig. 2C). For a quantitative evaluation, the ratio of the G_{1-59} resonance peak intensities [I(G_{1-59} free)/I(G_{1-59} bound)] was calculated at a molar ratio of 0.5, G_{1-59} to *d* subunit (Fig. 2D). Intensity changes were observed for residues Gly7-Lys34, whereby largest intensity changes were detected for the backbone amides of residues Ala9, Leu11, Glu15, Lys16, Ala18, His19, Val22 and Ala25. All these residues are located on

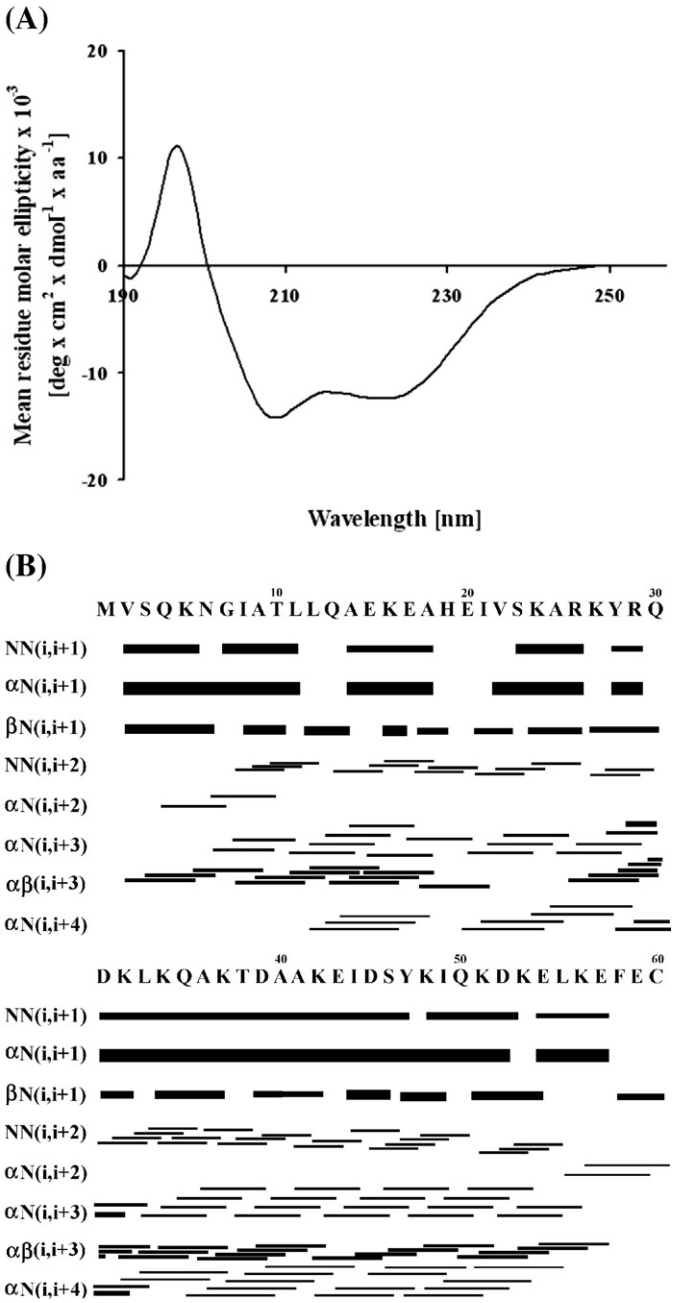

Fig. 4. (A) Far UV-CD spectrum of G_{1-59} of the V-ATPase from yeast. (B) Connectivity diagram of G_{1-59}. The line thickness reflects the intensities of the NOE connectivities.

the N-terminal segment of the G_{1-59} suggesting that the N-terminus forms the recognition site for G_{1-59} in its interaction with *d* subunit.

3.2. Real time binding studies of G_{1-59}–d by surface plasmon resonance G_{1-59}

Surface plasmon resonance (SPR) biosensors permit the real time monitoring of macromolecular interactions. Binding of molecules to the sensor surface generates a response which is proportional to the refractive index which is affected by the bound mass [29]. Immobilized subunit *d* on the sensor chip surface was used to study binding affinity kinetics with G_{1-59}. An association rate constant k_a=4.1 (±0.2)×10^5 M^{-1} s^{-1} and dissociation rate constant k_d=5.5 (±0.4)×10^{-4} s^{-1} were obtained (Fig. 3). Consequently dissociation constant (k_d/k_a) of K_D=1.3 (±0.3)×10^{-9} M was determined for binding between subunit *d* and G_{1-59}. The chi^2 was within 3.5% of R_{max} from the fit.

3.3. Solution structure of G_{1-59}

As G_{1-59} is forming the domain for G–*d* assembly, its structure elucidation came into the focus. The secondary structure of G_{1-59} was determined from circular dichroism spectra, measured between 190 and 260 nm (Fig. 4A). The minima at 222 and 208 nm and the maximum at 192 nm indicate the presence of α-helical structures in the protein. The average secondary structure content was 73% α-helix and 27% random coil. Two- and three dimensional NMR experiments have been performed to observe the solution structure of this protein. The structure of G_{1-59} was calculated on the basis of a total 565 nontrivial NMR-derived distance restraints. Hydrogen bonds were identified from the characteristic patterns of homonuclear ^{1}H nuclear Overhauser enhancements (NOEs) [23,30] and were introduced at the end of structure calculations. Typical α-helical NOE pattern, $d_{\alpha N}$ (*i*, *i*+3), $d_{\alpha N}$ (*i*, *i*+4) and $d_{\alpha\delta}$ (*i*, *i*+3), were observed from the amino acid residues 14 to 56 (Fig. 4B). Fig. 5A shows the overlay of the 10 lowest energy structures of G_{1-59} and the structural statistics are given in the Table 1. These structures have an overall RMSD of 0.87 Å for the backbone atoms and 1.42 Å for all the

Table 1
Structural statistics for the 10 selected structures of G_{1-59} of V-ATPase

Total number of NMR restraints	565
Number of unambiguous NOE peaks	
Intraresidual (|*i*−*j*|=0)	173
Sequential (|*i*−*j*|=1)	165
Medium-range (2≤|*i*−*j*|≤5)	84
Long-range (|*i*−*j*|>5)	0
Number of dihedral angle constraints	104
Number of hydrogen-bond distance restraints	39
Number of restraint violations	
Total number of restraint violations >0.3 Å	0
Total number of dihedral angle violations >5 Å	0
Ramachandran plot statistics (%)	
Fractions of residues of most favored regions (%)	94.7
Fractions of residues in additionally allowed regions (%)	5.3
Fractions of residues in generously allowed regions (%)	0
Fractions of residues in disallowed regions (%)	0
Structural precision of well ordered region	
RMSD backbone (residues (10–56)	0.87 Å
RMSD heavy (residues 10–56)	1.42 Å

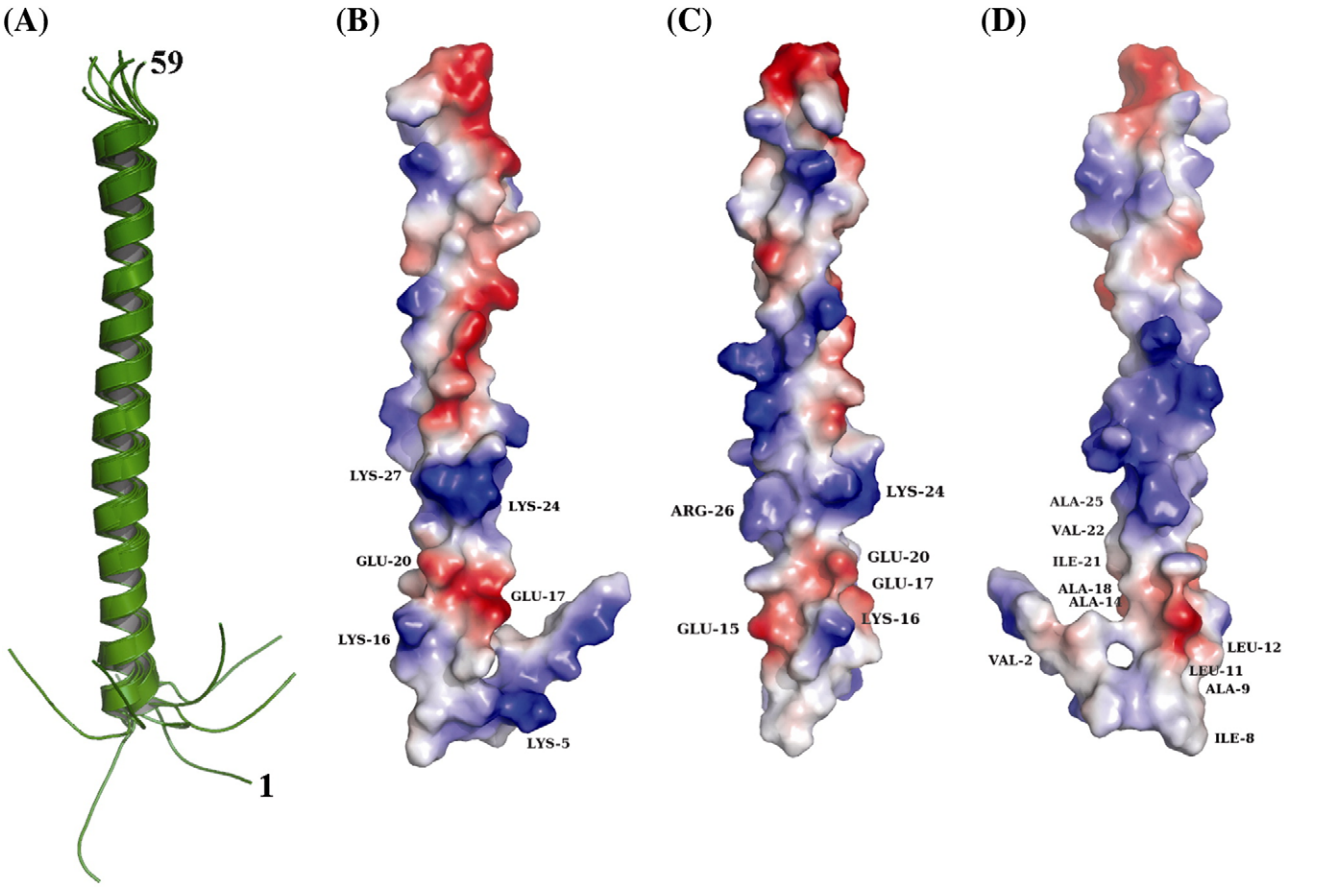

Fig. 5. Ribbon diagram of the NMR solution structure of G_{1-59}. (A) Best fit superimposition of the 10 lowest-energy NMR structures. (B–D) Different orientations of G_{1-59}, showing the molecular surface with the electrostatic potential of the peptide, drawn in PyMol [44] that uses Poisson–Boltzmann equation, where the positive potentials are drawn in blue and negative in red.

heavy atoms in the helical region of the three dimensional structures (residue 10–56) of the protein. All these structures have energies lower than 4 kcal mol^{-1}, with no NOE violations greater than 0.3 Å, and no dihedral violations greater than 5 Å. The protein has an extended helical structure from the residues Thr10 to Ala56 measuring a length of 67.9 Å excluding the unstructured region in the N- (1–9) and C- (57–59) terminal ends, as predicted from the amino acid sequence. Relaxation rates of NMR signals have been used to probe internal dynamics of the protein on ps to ns time-scale, revealing sensitivity to the motions. Backbone ^{15}N relaxation parameters R_1 and R_2 have been measured for the protein G_{1-59}. The average value of R_1 is 384 ms and R_2 is 166 ms (figure not shown). The relatively lower R_2 values observed in the terminal region of the protein indicate that there are faster internal motions as compared to the central region of this helical protein G_{1-59}. The surface charge distribution on one side of G_{1-59} exhibits a strip of negative amino acids at the C-terminus, whereby its N-terminus has a more amphiphilic character due to positive and negative charge distribution, attributed by the residues Lys5, Lys16, Lys24, Arg26 and Lys27 and Glu15, Glu17, Glu20, respectively (Fig. 5A–B). On the opposite side the structure of G_{1-59} reveals a hydrophobic surface at the N-terminus, made-up by the residues Val2, Ile8, Ala9, Leu11, Ala14, Ala18, Ala25 and Val22 (Fig. 5C).

3.4. Model for the interface of G_{1-59}/E_{18-38} complex

Recent NMR-titration experiments demonstrated that subunit G and E are interacting via the residues Met1, Val2, Ser3, Lys5, Val22, Ser23, Lys24, Ala25 and Arg26 of G_{1-59} as well as the amino acids of the segment E_{18-38} of subunit E (18). In these studies the three dimensional NMR solution structure of the segment E_{18-38} of yeast V-ATPase was solved [18]. With these data and the presented solution structure of G_{1-59} in hand we have now docked the helical peptide, E_{18-38}, with G_{1-59} iteratively maximizing favorable interactions between the exposed side chains (see Materials and methods). The best docking model was chosen as explained in the experimental section and its docking energy was calculated to be −164.58 kJ/mol using the formula, Docking energy = Energy of the G_{1-59}–E_{18-38} Complex − (Energy of the subunit G_{1-59} + Energy of the subunit E_{18-38}); where the final minimized energies of the G_{1-59}–E_{18-38} complex, subunit G_{1-59} and the subunit E_{18-38} are −4619.48, −3336.456 and −1118.44 kJ/mol, respectively. The detailed interaction between the best docked complex configurations is shown in Fig. 7. From the docked structure it could be observed that the complex is stabilized by two binding regions, one near the N-terminals of the two subunits and the other in the middle (Val22–Arg26) of the G subunit helix, which is interacting with the hinge region of the E_{18-38} peptide. The N-terminal binding is mostly stabilized by polar strong interactions whereas the second binding region is mostly stabilized through weak hydrogen bonding and van der Waals forces. It could be inferred that in the N-terminal binding region, the main chain carbonyl of Met1 of G_{1-59} forms a hydrogen bond with main chain nitrogen atom of Asn18 of E_{18-38} peptide. In addition the side chain oxygen atom of Ser3 of G_{1-59} has hydrogen bond interaction with the side chain nitrogen of Lys19 of E_{18-38}. In the second binding region, specific interaction is noted for Val22 of G_{1-59} wherein its side chain carbon atom has weak hydrogen bonding interaction with the side chain oxygen atom of Glu29 of E_{18-38} peptide in the model. The other few residues such as Ser23, Lys24, Ala25 and Arg26 confer stability to the complex through weak van der Waals forces.

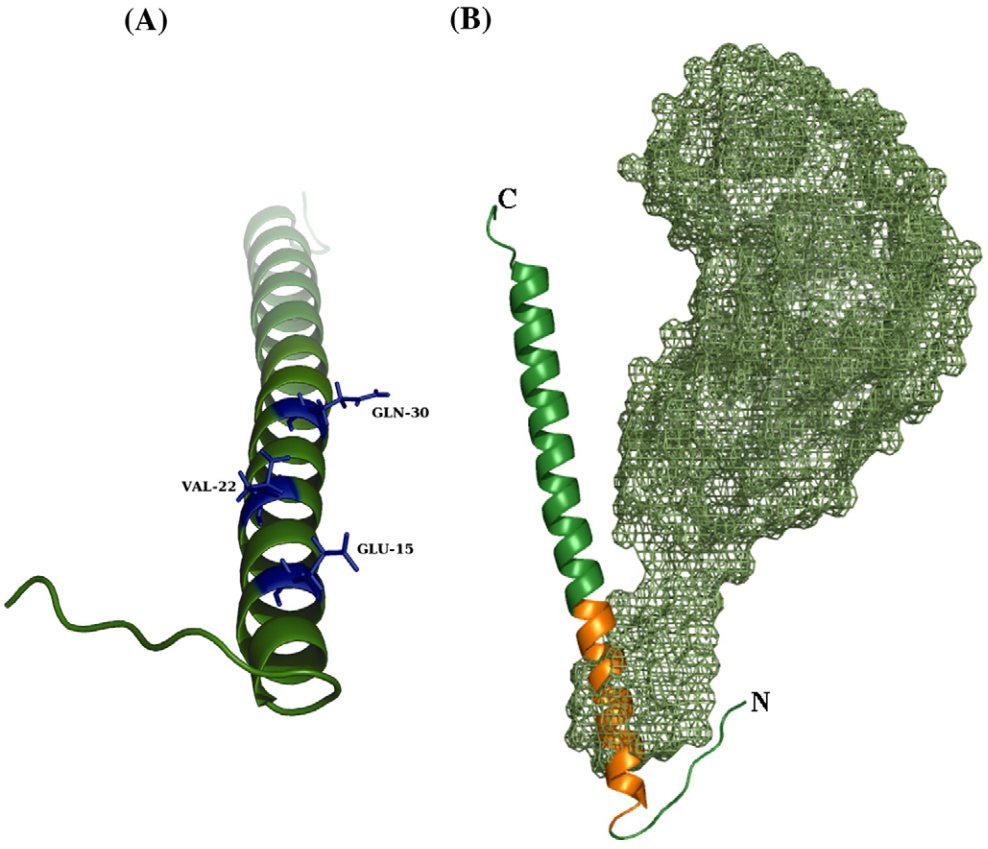

Fig. 6. (A) Ribbon diagram of the NMR solution structure of G_{1-59} illustrating the relative positions of residues Glu15, Val22 and Gln30 inside the α-helix, which are marked in blue color. (B) A model showing the interaction between subunits G (G_{1-59}, green) and *d* (smudge). The low resolution structure of subunit *d* from yeast (9) (surface representation) and the average NMR structure of G_{1-59} (cartoon representation) is used for the modeling. The binding region (Ala9 to Ala25) of G_{1-59} is highlighted in orange color.

4. Discussion

The G subunit has been reported to be present in multiple copies of the V_1V_O ATPase of bovine cells [15] and *S. cerevisiae* [16]. Quantitative analysis has indicated that bovine clathrin-coated vesicle enzyme contains two copies of subunit G per V-ATPase and that in the yeast enzyme subunit G has a stoichiometry of two to three [14–16]. Subunit G is required for proton pumping catalyzed by the V_1V_O complex [31–33], ATPase activity [33–36] and V_1V_O assembly [32]. In this canon, subunit G is described to be strongly associated with the nucleotide-binding subunit B and also weakly with subunit A of the catalytic V_1 sector [14] as well as with the stalk subunit E [14,18,19] and subunit *d* of the V_O sector [14], which represent different domains of actions. Precipitation assays revealed that subunit G associates with subunit *d* (Vma6p) from *S. cerevisiae* V-ATPase [14]. The presented NMR data enables the identification of residues Gly7 to Lys34 of subunit G, involved in the binding with subunit *d* (Fig. 2B). No binding could be detected, when the ^{15}N labeled G_{61-114} has been titrated with subunit *d*, indicating that the subunit *d* binds only via the N-terminal segment of subunit G. The NMR-titration experiments and the charge distribution of the G_{1-59} structure (Fig. 5B–D) implies that the G–*d* binding occurs via the more hydrophobic epitope at the very N-terminus, characterized by the residues Val2, Ile8, Ala9, Leu11, Ala14, Ala18, Val22 and Ala25 as well as with a charged segment, formed by the amino acids Lys16, Glu15, Glu17, Glu20, Lys24, Arg26, Lys27 and Asp31 (Fig. 5B). Amino acid substitution of subunit G residues Glu15 to Ala and deletions of Val22 and Asp31, respectively, exhibited loss in ATPase activity [32]. The structure of G_{1-59} shows that these residues form a strip (Fig. 6A). Therefore, substitution or deletion of one of these residues might cause a weaker interaction of both subunits G and *d*. Although G_{1-59} makes up only a segment of subunit G, the binding constant (K_D = 1.3 (±0.3)× 10^{-9} M) of G_{1-59}–*d* determined, which might be lower in the entire enzyme, is in line with two subunits being in close neighborhood inside the entire V_1V_O ATPase.

Solution X-ray scattering data revealed that G is elongated [17], with a proposed α-helical and highly conserved N-terminal half [37]. The NMR solution structure of the N-terminal domain, G_{1-59}, of subunit G yields an extended helical structure from the residues Thr_{10} to Ala_{56} with a length of 67.9 Å, indicating that the entire subunit G might be able to bridge the distances between the two sectors of the V_1V_O ATPase complex. Also extended is subunit *d* from *S. cerevisiae* V-ATPase with 11 nm in length [9]. The low resolution structure of subunit *d* from yeast in solution shows a boxing glove-shaped molecule, consisting of a major globular domain and a protuberance (Fig. 6B; [9]). A structural comparison with the 3D-reconstruction of the V-sector showed that *d* is connected via its protuberance to the N-terminus of subunit *a* [9,12]. In parallel, subunit *d* does bind to the major subunit A as shown by fluorescence correlation spectroscopy and surface plasmon resonance (unpublished data). While the globular domain of *d* is bound to A, the protuberance of *d*, which is partially in neighborhood to subunit *a* [9,12], becomes accessible for the assembly with the N-terminus of one of the G subunits (Fig. 6B). This would orient the remaining C-terminal half of G close to subunit A and B, as G is shown to bind subunit A and B [14].

Biochemical data with truncated forms of subunit E of the yeast V-ATPase have shown that deletions of the N-terminal 38 residues (E_{39-233}) and 110 amino acids ($E_{110-233}$) results in a complete loss of E–G association, whereby the truncations of the first 19 residues or the C-terminal amino acids 112–233 (E_{1-112}) did not alter the binding traits of both subunits, suggesting that the N-terminal region 19 to 38 of subunit E might interact with subunit G [14]. NMR- and fluorescence correlation spectroscopy results confirmed

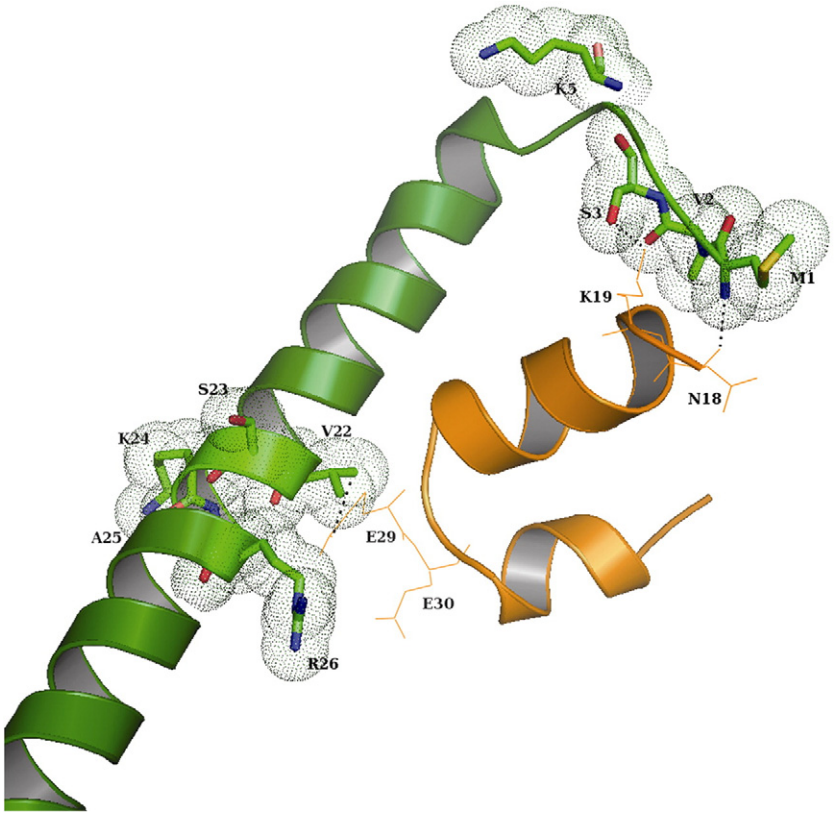

Fig. 7. The docked complex of the determined NMR structures of G_{1-59} (green) and E_{18-38} ([18], orange). The residues shown in stick representation with dotted surface in the G_{1-59} are the ones that are shown by NMR titration experiments [18] to have binding (M1, V2, S3 and K5; V22, S23, K24, A25 and R26). The residues in peptide E_{18-38} that reveal polar contacts (black dotted lines) with G_{1-59} are shown in stick representation.

this data and allowed the identification of amino acids Met1, Val2, Ser3, and Lys5 as well for Val22, Ser23, Lys24, Ala25 and Arg26 of subunit G in the assembly of E_{18-38} [18], and moreover, together with the biochemical data published by Jones et al. [14], excluded that E and G form a coiled-coiled interaction over the length of both molecules as proposed recently [16]. The solution structure of E_{18-38} reveals a helix–hinge–helix arrangement in which both helices are separated by 119° and the C-terminal helix is bend in the *z*-axis relative to the N-terminal one (Fig. 7; [18]). Most recently, we used a model of G_{1-59} for docking to the solution structure of E_{18-38} [18], and in that we could infer that most of the residues of G_{1-59} which show shift in their HSQC spectrum also had some kind of interaction with the E_{18-38} peptide. The large shifts of the subunit G could be explained by the strong hydrogen bonding interactions. In the similar way we now used the determined NMR structure of G_{1-59} instead of the modeled one to dock with the solution structure of E_{18-38} and the docking energy for the complex was calculated to be −164.58 kJ/mol indicating tighter binding. From the best docked model we noted two binding regions, and most of the residues of the G subunit which were identified to interact with the E_{18-38} peptide from the NMR titration experiments [18] are found within a radius of 6 Å in the complex. The HSQC spectrum showed relatively larger shifts for residues Met1 and Arg26 of subunit G. In the docked model the Met1 residue has strong hydrogen bonding interaction with Asn18 of the E peptide and this explains the relatively larger shift. However, the residue Arg26 of G_{1-59} which also shows large shift in the spectrum is not found to have any strong interaction in the proposed model. This could be explained due to the side chain flexibility of the Arg residue that could take many different low energy conformations. So during *in vivo* protein–protein complex formation it might orient in such a way that it interacts with the side chains of Glu29 and/or Glu30 of E_{18-38}. The spectral shift observed for the residues Ser3 and Val22 of G_{1-59} [18] could be attributed to their hydrogen bonding interactions with Lys19 and Glu29 of E_{18-38}, respectively, whereby the shift for the other residues Ser23, Lys24, Ala25 and Val2 of G_{1-59} could be caused by van der Waals interactions that they have with Glu29, Glu30 and Met20 of the E_{18-38} peptide (Fig. 7).

The number of the V_1 ATPase stalk subunits E, G and H with copy numbers of 2–3 [14,15,38], 2–3 [14,15,38] and 1–2 [39,40], respectively, is a matter of debate. In comparison the stoichiometry of one for the subunits C, D, F and the V_O subunits *a* and *d* is defined [40]. Subunit *d*, with a copy number of one, does bind to segment Gly7 to Lys34 of subunit G. The N-terminal part Met1 to Lys5 as well for Val22 to Arg26 of G binds via the amino acids E_{18-38} to subunit E. In parallel, the first 18 N-terminal residues of subunit E interact with one subunit C [14], whereas the 78 amino acid domain of E is required for assembly with subunit H [41]. In summary, these phenomena indicate that the two or three copies of G and E subunits, respectively, have different binding partners in their N-terminal parts, implying different roles inside the V_1V_O complex. The variety of binding partners of G and/or E might explain the multiple functions of both subunits in ATP hydrolysis [33–36], proton transport [31,42] and V_1V_O assembly [38,43].

Acknowledgements

This research was supported by the School of Biological Sciences, NTU. S. Rishikesan, S. Gayen and Y.R. Thaker are grateful to the authority of Nanyang Technological University (NTU) for awarding research scholarship.

References

[1] K.W. Beyenbach, H. Wieczorek, The V-type H^+ ATPase: molecular structure and function, physiological roles and regulation, J. Exp. Biol. 209 (2006) 577–589.
[2] V. Marshansky, M. Futai, The V-type H+-ATPase in vesicular trafficking: targeting, regulation and function, Cur. Opin. Cell. Biol. 20 (2008) 415–426.
[3] J.S. Lolkema, Y. Chaban, E.J. Boekema, Subunit composition, structure, and distribution of bacterial V-Type ATPase, J. Bioenerg. Biomembr. 35 (2003) 323–336.
[4] S. Saroussi, N. Nelson, Vacuolar H^+-ATPase—an enzyme for all seasons, Pflugers Arch — Eur. J. Physiol. Eur. J. Physiol. 457 (2009) 581–587.
[5] G. Grüber, V. Marshanski, New insights into structure–function relationships between archeal ATP synthase (A_1A_O) and vacuolar type ATPase (V_1V_O), Bioessays 30 (2008) 1096–1099.
[6] T. Inoue, S. Wilkens, M. Forgac, Subunit structure, function and arrangement in the yeast and coated vesicle V-ATPase, J. Bioenerg. Biomembr. 35 (2003) 291–299.
[7] G.-H. Sun-Wada, Y. Wada, M. Futai, Vacuolar H+ pumping ATPase in luminal acidic organelles and extracellular compartments: common rotational mechanism and diverse physiological roles, J. Bioenerg. Biomembr. 35 (2003) 347–358.
[8] S. Wilkens, Z. Zhang, Y. Zheng, A structural model of the vacuolar ATPase from transmission electron microscopy, Micron. 36 (2005) 109–126.
[9] Y.R. Thaker, M. Roessle, G. Grüber, The boxing glove shape of subunit *d* of the yeast V-ATPase in solution and the importance of disulfide formation for folding of this protein, J. Bioenerg. Biomembr. 39 (2007) 275–289.
[10] T. Nishi, S. Kawasaki-Nishi, M. Forgac, Expression and function of the mouse V-ATPase *d* subunit isoforms, J. Biol. Chem. 278 (2003) 46396–46402.
[11] G.I. Miura, G.J. Froelick, D.J. March, K.L. Stark, R.D. Palmiter, The *d* subunit of the vacuolar ATPase (ATP6d) is essential for embryonic development, Transgenic. Res. 12 (2003) 131–133.
[12] S. Wilkens, M. Forgac, Three-dimensional structure of the vacuolar ATPase proton channel by electron microscopy, J. Biol. Chem. 276 (2001) 44064–44068.
[13] C. Bauerle, M.N. Ho, M.A. Lindorfer, T.H. Stevens, The *Saccharomyces cerevisiae* vma6 gene encodes the 36-kDa subunit of the vacuolar H^+-ATPase membrane sector, J. Biol. Chem. 268 (1993) 12749–12757.
[14] R.P.O. Jones, L.J. Durose, J.B.C. Findlay, M.A. Harrison, Defined sites of interaction between subunit E (Vma4p), C (Vma5p), and G (Vma10p) within the stator structure of the vacuolar H^+-ATPase, Biochemistry 44 (2005) 3933–3941.
[15] T. Xu, E. Vasilyeva, M. Forgac, Subunit interactions in the clathrin-coated vesicle vacuolar (H^+)–ATPase complex, J. Biol. Chem. 274 (1999) 28909–28915.
[16] N. Kitagawa, H. Mazon, A.J.R. Heck, S. Wilkens, Stoichiometry of the peripheral stalk subunits E and G of yeast V_1-ATPase determined by mass spectrometry, J. Biol. Chem. 283 (2008) 3329–3337.
[17] A. Armbrüster, S.M. Bailer, M.H.J. Koch, J. Godovac-Zimmermann, G. Grüber, Dimer formation of subunit G of the yeast V-ATPase, FEBS Lett. 546 (2003) 395–400.
[18] S. Rishikesan, Y.R. Thaker, R. Priya, S. Gayen, M.S.S. Manimekalai, C. Hunke, G. Grüber, Mol. Membr. Biol. 25 (5) (2008) 400–410.
[19] J. Féthière, D. Venzke, D.R. Madden, B. Böttcher, Peripheral stator of the yeast V-ATPase: stoichiometry and specificity of interaction between the EG complex and subunit C and H, Biochemistry 44 (2005) 15905–15914.
[20] U.K. Laemmli, Cleavage of structural proteins during the assembly of the head of bacteriophage T4, Nature 227 (1970) 680–685.
[21] D.G. Kneller, T.D. Goddard, SPARKY 3.105 edit, University of California, San Francisco, CA, 1997.
[22] M.V. Berjanskii, S. Neal, D.S. Wishart, PREDITOR: a web server for predicting protein torsion angle restraints, Nucleic Acids Res. 34 (2006) 63–69.
[23] K. Wüthrich, NMR of Proteins and Nuclei Acids, Wiley, Interscience, New York, 1986.
[24] T. Herrmann, P. Güntert, K. Wüthrich, Protein NMR structure determination with automated NOE assignment using the new software CANDID and the torsion angle dynamics algorithm DYANA, J. Mol. Biol. 319 (2002) 209–227.
[25] B. Johnson, S. Lofas, G. Lindquist, Immobilization of proteins to a carboxyldextran-modified gold surface for biospecific interaction analysis in surface plasmon resonance sensors, Analytical Biochemistry 198 (1991) 268–277.
[26] A. Tovchigrechko, I.A. Vakser, GRAMM-X public web server for protein–protein docking, Nucleic Acids Res. 34 (2006) 310–314.
[27] N. Guex, M.C. Peitsch, SWISS-MODEL and the Swiss-PdbViewer: an environment for comparative protein modeling, Electrophoresis 18 (1997) 2714–2723.
[28] L.E. Kay, D.R. Muhandiram, N.A. Farrow, Y. Aubin, J.D. Forman-Kay, Correlation between dynamics and high affinity binding in an SH2 domain interaction, Biochemistry 35 (1996) 361–368.
[29] M. Fivash, E.M. Towler, R.J. Fisher, BIAcore for macromolecular interaction, Curr Opin Biotechnol, 9 (1998) 97–101.
[30] K. Wüthrich, G. Wider, G. Wagner, W. Braun, Sequential resonance assignments as a basis for determination of spatial protein structures by high resolution proton nuclear magnetic resonance, J. Mol. Biol. 155 (1982) 311–319.
[31] J.J. Tomashek, B.S. Garrison, D.J. Klionsky, Reconstitution *in vitro* of the V_1 complex from the yeast vacuolar proton-translocating ATPase. Assembly recapitulates mechanism, J. Biol. Chem. 272 (1997) 26787–26793.
[32] C.M.H. Charsky, N.J. Schumann, P.M. Kane, Mutational analysis of subunit G (Vma10p) of the yeast vacuolar H^+-ATPase, J. Biol. Chem. 275 (2000) 37232–37239.
[33] B.P. Crider, P. Andersen, A.E. White, Z. Zhou, X. Li, J.P. Mattson, L. Lundberg, D.J. Keeling, X.S. Xie, D.K. Stone, S.B. Peng, Subunit G of the vacuolar proton pump. Molecular characterization and functional expression, J. Biol. Chem. 272 (1997) 10721–10728.
[34] J.J. Tomashek, L.A. Graham, M.U. Hutchins, T.H. Stevens, D.J. Klionsky, V_1-situated stalk subunits of the yeast vacuolar proton-translocating ATPase, J. Biol. Chem. 272 (1997) 26787–26793.
[35] R. Gräf, W.R. Harvey, H. Wieczorek, Purification and properties of a cytosolic V_1-ATPase, J. Biol. Chem. 271 (1996) 20908–20913.
[36] V.F. Rizzo, Ü. Coskun, M. Radermacher, T. Ruiz, A. Armbrüster, G. Grüber, Resolution of the V_1-ATPase from *Manduca sexta* into subcomplexes and

visualization of an ATPase active A_3B_3EG-complex by electron microscopy, J. Biol. Chem. 278 (2003) 270–275.
[37] I.E. Hunt, B.J. Bowman, The intriguing evolution of the "b" and "G" subunit in F-type and V-type ATPase: isolation of the *vma*-10 gene from *Neurospora crassa*, J. Bioenerg. Biomembr. 29 (1997) 533–540.
[38] M. Ohira, A.M. Smardon, C.M. Charsky, J. Liu, M. Tarsio, P.M. Kane, The E and G subunits of the yeast V-ATPase interact tightly and are both present at more than one copy per V1 complex, J. Biol. Chem. 281 (2006) 22752–22760.
[39] Z. Zhou, S.B. Peng, B.P. Crider, P. Anderson, X.S. Xie, D.K. Stone, Recombinant SFD isoforms activate vacuolar proton pumps, J. Biol. Chem. 274 (1999) 15913–15919.
[40] L.A. Graham, A.R. Flannery, T.H. Stevens, Structure and assembly of the yeast V-ATPase, J. Bioenerg. Biomembr. 35 (2003) 301–312.
[41] M. Lu, S. Vergara, L. Zhang, L.S. Holliday, J. Aris, S.L. Gluck, The amino-terminal domain of the E subunit of vacuolar H(+)-ATPase (V-ATPase) interacts with the H subunit and is required for V-ATPase function, J. Biol. Chem. 277 (2002) 38409–38415.
[42] G.-H. Sun-Wada, Y. Imai-Senga, A. Yamamoto, Y. Murata, T. Hirata, Y. Wada, M. Futai, A proton pump ATPase with testis-specific E1-subunit isoform required for acrosome acidification, J. Biol. Chem. 277 (2002) 18098–18105.
[43] K. Hayashi, G.-H. Sun-Wada, Y. Wada, M. Nakanishi-Matsui, M. Futai, Defective assembly of a hybrid vacuolar H(+)-ATPase containing the mouse testis-specific E1 isoform and yeast subunits, Biochem. Biophys. Acta 1777 (2008) 1370–1377.
[44] W.L. DeLano, The PyMol Molecular Graphics System, DeLano Scientific, San Carlos, CA, 2001.